

# **MULLITIZATION BEHAVIOUR OF ALUMINA ENRICHED CLAY IN PRESENCE OF DOPANT $\text{Fe}_2\text{O}_3$**

A Thesis Submitted  
In Partial Fulfilment of the Requirement  
For the degree of  
**BACHELOR OF TECHNOLOGY**

BY  
**HARAPRASAD RAUT**  
ROLL NO 108CR047



TO THE  
  
DEPARTMENT OF CERAMIC ENGINEERING  
NATIONAL INSTITUTE OF TECHNOLOGY ROURKELA  
  
MAY 2012

## **CERTIFICATE**

This is certified that the work contained in the project entitled “**MULLITIZATION BEHAVIOUR OF ALUMINA ENRICHED CLAY IN PRESENCE OF DOPANT  $\text{Fe}_2\text{O}_3$** ” by Haraprasad Raut (Roll 107CR047) in partial fulfilment of the requirements of the award of Bachelor of Technology Degree in Ceramic Engineering at the National Institute of Technology, Rourkela is an authentic work carried out by her under my supervision and guidance. To the best of my knowledge, the matter embodied in the thesis has not been submitted to any other university / institute for the award of any Degree or Diploma.

SUNIPA BHATTACHARYYA

DEPARTMENT OF CERAMIC ENGINEERING

NATIONAL INSTITUTE OF TECHNOLOGY

ROURKELA – 769008

## **ACKNOWLEDGEMENT**

I express my deep gratitude to my guide, Prof S. Bhattacharyya, Department of Ceramic Engineering, N I T Rourkela, for his valuable advice, time and guidance in the completion of this project work. My heartfelt thanks to all the faculty members for their suggestions during this project work. My sincere acknowledgement to the Research Scholars, M. Tech students and the non-teaching staff for the help and cooperation extended to us. And finally, my hearty thanks to all my friends who have constantly helped me.

HARAPRASAD RAUT

ROLL NO – 108CR047

Figure	FIGURE CAPTION	Page No.
Fig 1	Alumina and Silica phase diagram	12
Fig 2	EDTA structure	17
Fig 3	Mixing of china clay in the pot mill	18
Fig 4(a,b)	(a) Mixed sample, (b) Dried sample after 2 days	20
Fig 5	Fired sample picture	22
Fig 6	Diametric compression test ( loading and fracture mode)	25
Fig 7	DSC and TG plot of the china clay	28
Fig 8	Bulk density vs Temperature	29
Fig 9	Bulk density vs % Fe <sub>2</sub> O <sub>3</sub>	29
Fig 10	AP vs temperature	30
Fig 11	AP vs % Fe <sub>2</sub> O <sub>3</sub>	31
Fig 12	Linear shrinkage vs Temperature	31
Fig 13	linear shrinkage vs % Fe <sub>2</sub> O <sub>3</sub>	32
Fig 14	BET surface area plot	32
Fig 15	XRD of china clay calcined at 1000 <sup>0</sup> C	34
Fig 16	XRD of reactive alumina	34
Fig 17	XRD analysis of the 0% Fe <sub>2</sub> O <sub>3</sub>	35
Fig 18	XRD analysis of the 3% Fe <sub>2</sub> O <sub>3</sub>	35
Fig 19	XRD analysis of the 4.5% Fe <sub>2</sub> O <sub>3</sub>	36
Fig 20	XRD analysis of the 6% Fe <sub>2</sub> O <sub>3</sub>	36
Fig 21	XRD analysis of 0% Fe <sub>2</sub> O <sub>3</sub> ,3% Fe <sub>2</sub> O <sub>3</sub> ,4.5% Fe <sub>2</sub> O <sub>3</sub> , 6% Fe <sub>2</sub> O <sub>3</sub> fired at 1650 <sup>0</sup> C	37
Fig 22	XRD analysis of 0% Fe <sub>2</sub> O <sub>3</sub> ,3% Fe <sub>2</sub> O <sub>3</sub> ,4.5% Fe <sub>2</sub> O <sub>3</sub> , 6%	38

	Fe <sub>2</sub> O <sub>3</sub> samlpes fired at 1650 <sup>0</sup> C are plotted in range 2 $\Theta$ (25-30)	
Fig 23(a)	SEM image of 0% Fe <sub>2</sub> O <sub>3</sub> (X15000)	39
Fig 23(b)	SEM image of 0% Fe <sub>2</sub> O <sub>3</sub> (X7500)	39
Fig 24	SEM image of 3% Fe <sub>2</sub> O <sub>3</sub> (X1500)	40
Fig 25(a)	SEM image of 4.5% Fe <sub>2</sub> O <sub>3</sub> (X1500)	40
Fig 25(b)	SEM image of 4.5% Fe <sub>2</sub> O <sub>3</sub> ( X3500)	40
Fig 26	SEM image of 6% Fe <sub>2</sub> O <sub>3</sub> ( X1500)	41

CONTENTS	Page No
Certificate	2
Acknowledgment	3
List of figure	5
Abstract	7
Chapter 1	
Introduction	9
Chapter 2	
Literature Review	12
Chapter 3	
Experimental work	16
Chapter 4	
Experimental characteristic	23
Chapter 5	
Results and Discussion	27
Chapter 6	
Conclusion	42
Chapter 7	
Scope of future work	44
Reference	46

## ABSTRACT

Mullatization behaviour of china clay with reactive alumina sources has been studied. The calcined clay was ground then mixed with reactive alumina. These raw material are mixed with different amount of iron oxide (vig. 0%  $\text{Fe}_2\text{O}_3$ , 1.5%  $\text{Fe}_2\text{O}_3$ , 3%  $\text{Fe}_2\text{O}_3$ , 4.5%  $\text{Fe}_2\text{O}_3$ , 6%  $\text{Fe}_2\text{O}_3$ ). Rectangular bars and pallets were sintered at different temperatures (vig.  $1450^\circ\text{C}$ ,  $1550^\circ\text{C}$ ,  $1650^\circ\text{C}$ ) with a soaking period of 2 hrs. A holding in temperature was done to accommodate binder burn out. Previously the characterizations of the raw materials were carried by XRD analysis, DSC, TG. The X-ray and microstructural analysis were to understand the mullatization behaviour of the china clay. The calcined clay derived samples were used as they show better physical and mechanical properties and it shows very low shrinkage. The fired samples fired at  $1650^\circ\text{C}$  shows more than 98% mullite formation in the body but they differ in their grain size. With increase in the percentage iron oxide there is not significant change in the formation in the mullite formation at  $1650^\circ\text{C}$  but the grain size increases continuously. The formation of needle like mullite grain increases with increases in the iron oxide content. With increase in the iron oxide content there is decrease in the amount in the unreacted free alumina. Microstructural studies on the sintered and polished samples and X-ray diffraction studies on the sintered specimens are carried out to estimate the mullitization of the individual samples fired at different temperatures. The formation of secondary mullite formation has been observed through inter-diffusion. The formation of primary mullite formation has been observed at lower iron oxide content through XRD analysis.

# CHAPTER 1

## INTRODUCTION



## 1.1 Introduction

In the recent decade there has been continuous work is going on the mullite powder and mullite body preparation. This much high interest on the mullite in the conventional and advanced ceramic body preparation is due to its unique properties in the field of structural and electrical field. It has very low density i.e  $3.17 \text{ g cm}^{-3}$ , low thermal conductivity  $k = 2.0 \text{ Wm}^{-1}\text{K}^{-1}$ , low thermal expansion coefficient, low dielectric constant and excellent mechanical properties at high temperature <sup>[15]</sup>. Mullite can be prepared from different methods like solid state reaction, Hydrothermal, Co-precipitation, Sol-gel method. There has been extensive work on preparation of mullite through the cost effective way and getting the high percentage of mullite formation. When purity matters and the cost effectiveness matters mullite preparation from the firing of the alumina enriched china clay with some dopant like iron oxide and chromium oxide is preferred. To prepare high purity mullite high cost raw material are required so due to high cost some of the above processes are not preferred as bulk amount cannot be prepared from this method <sup>[16]</sup>. Kaolinite, which belongs to the kaolin group ( $\text{Al}_2 \text{Si}_2\text{O}_5 \cdot 4(\text{OH}) \cdot 2\text{H}_2\text{O}$ ), has perhaps been the most popular clay in this research field, with other clays of interest including halloysite (kaolin group), kyanite, *etc.* Fine mullite grains may be obtained from halloysite sintering <sup>[17]</sup>. There has been observation of significant cracking due to the coexisting phase like cristobalite which we are going to eliminate in the following work. In kaolinite alumina system, kaolinite first dehydrated to Meta kaolinite in the temperature range  $400^\circ\text{C}$ - $500^\circ\text{C}$ . It has been observed that below  $1300^\circ\text{C}$  the major reaction is the kaolinite series reaction which converts into primary mullite and the cristobalite phase, amorphous silica and the reactive alumina remains unreacted. It acts as an inert material below  $1300^\circ\text{C}$  <sup>[18]</sup>. As the temperature rose above the  $1400^\circ\text{C}$  the transitory liquid phase reacts with the extra alumina added which

forms the secondary mullite phase. The reaction rate is very slow till the temperature goes up to  $1555^{\circ}\text{C}$  and there has been an excessive fast reaction above  $1600^{\circ}\text{C}$  due to strong effect of eutectic liquid formation at temperature  $1595^{\circ}\text{C}$  <sup>[17]</sup>. The kaolinite and Meta kaolinite transformation proceeds very slow and Meta kaolinite has extremely very defective structure as it shows very volume lattice vacancies i.e. 20%. The vacancies are appeared due to the release of the lattice water present in that body. This the reason for low physical and chemical properties when used uncalcined clay as they leave very high vacancies the sintered body and it may happen that there may be damage in the body during firing. This is the reason calcined clay is preferred for body preparation as it shows better physical and mechanical properties with lower shrinkage in the body. Method of preparation of high purity mullite is:

1. Solid state interaction method
2. Sol-gel method
3. Hydrothermal method
4. Chemical vapour deposition

The above process yield pure mullite form but for large scale production it is not suitable due to high cost raw materials and processing technique. For large scale production we require low cost raw materials and atomic scale mixing. So clay remains the cheapest raw materials and cheapest raw material to form mullite by addition of extra alumina from outside.

# CHAPTER 2

# LITERATURE

# REVIEW

## 2.1 Literature Review

### 1. Secondary mullite:

By the addition of the reactive alumina, after formation of primary mullite it leaves out silica and an impurity containing silica rich liquid. These two will then react with the alumina to form secondary mullite upon further heating. The secondary mullite formation starts at a temperature above 1400°C. From the silica and alumina phase diagram (Fig 1) we get the first eutectic at 1595°C. By addition of dopants like  $\text{Fe}_2\text{O}_3$  it gives the eutectic at lower temp at around 1054-1150°C.

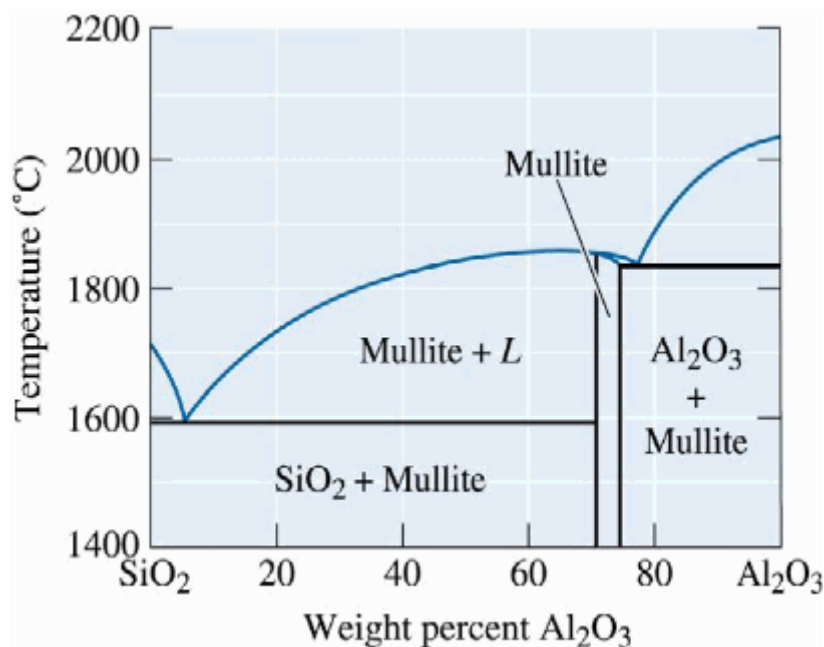


**Fig 1 Alumina and Silica phase diagram**

The entire precursors are produced with a chemical composition which corresponds to a stoichiometric mullite using different processing routes. The degree of mixing between Al and Si atoms in the non-crystalline mullite precursors at temperature just below the crystallization strongly influences the crystallization behaviour above 900°C. With starting material alumina and  $\text{SiCl}_4$  when mixed diluting and homogenised for 3 hour hydrolysis was carried out by addition of a mixture of water and isopropanol and molar ratio of water and alcohol is maintained 3:1. During hydrolysis formation of white flocculants and

release of white vapour have been observed. The sample prepared by above method contain very homogeneous network containing randomly distributed silica tetrahedral and alumina tetrahedral, octahedral, pentahedral. So the sample directly crystallises to mullite at temperature above 900<sup>0</sup>C. But the main draw back in this method is due to high cost of precursor and costly processing method and the driving force for crystallisation is instable due to present of pentahedraly coordinated Al at 900<sup>0</sup>C<sup>[17]</sup>.

## 2.2. Bimodal mullite crystal

Bimodal mullite crystal indicates the presence of secondary mullite. The mullite nucleation and primary mullite growth were observed in the sample fired at 1400<sup>0</sup>C. the rate of secondary mullite formation is very slow in presence of liquid phase. The kinetic of secondary mullite formation is very slow below temperature 1555<sup>0</sup>C. The coexisting liquid phase strongly suggests the solution precipitation via transitory liquid phase is major mechanism for secondary mullite formation.

Secondary mullite formation via solid state inter diffusion may occur in parallel but its contribution to secondary mullite formation but only can be regarded as minor.

By the X-ray line profile analysis it was possible to observe between 1300<sup>0</sup>C and 1550<sup>0</sup>C phases, simultaneous presence of two mullite morphologies and evolution of the crystallite size in both mullite morphologies.

XRD microstructural studies established that bimodal mullite crystals corresponding to secondary mullite nucleation and primary mullite growth were clearly observed at 1300<sup>0</sup>C at temperature 100<sup>0</sup>C than TEM studies carried out in the mullite obtained from alumina mixtures<sup>[19]</sup>.

## 2.3. Mechanism of Mullite formation

The mechanism of mullite formation generally includes 3 steps they are

- Solid states inter diffusion between silica and alumina<sup>[18]</sup>.

- The dissolution of alumina by a metastable eutectic liquid to form a transitory liquid phase followed by precipitation of mullite, the metastable eutectic liquid could be formed from silica and alumina at temperature greater than  $1200^{\circ}\text{C}$  <sup>[18]</sup>.
- The dissolution of alumina by the impurity silica containing silica rich liquid to form a transitory silica rich liquid to form a transitory liquid followed by the precipitation of mullite. The first impurity containing liquid could be appeared as early as  $985^{\circ}\text{C}$  with  $\text{K}_2\text{O}$  present in the system <sup>[18]</sup>.
- The secondary mullite formation is fastened in presence of iron oxide because  $\text{Fe}^{+3}$  replaces the  $\text{Al}^{+3}$  from its regular octahedral site and the free  $\text{Al}^{+3}$  replaces the  $\text{Si}^{+4}$  from its regular tetrahedral site which enhances the rate of reaction. This causes the elimination of unreacted alumina. So increasing the  $\text{Fe}_2\text{O}_3$  content there is decrease in the free alumina content <sup>[1]</sup>.

# CHAPTER 3

# EXPERIMENTAL

# WORK

### 3. Experimental Work

The raw materials used are china clay and industrial grade reactive alumina and iron oxide used as a dopant. Here PVA is used as a binder.

#### 3.1. Chemical Analysis of china clay

- About 0.5gm of the sample is mixed with 8-10gms of  $\text{Na}_2\text{CO}_3$  and 4-5 bits of NaOH and fused at  $800\text{-}1000^\circ\text{C}$  for 1 hour.
- Fused mass dissolved in 1:1 HCl and baked for overnight.
- After backing the residue was dissolved in the 1:4 HCl and filtered through Wattman 40 filter paper.
- From the residue we calculate the amount of  $\text{SiO}_2$ .
- The filtrate contains iron oxide which could be estimated by titrating with standard Mercurous nitrate solution using  $\text{NH}_4\text{HCN}$ .
- 10ml of filtrate is taken, few drops of methyl red indicator was added then liquid ammonia was added till the colour changes from pink to yellow. Then it is warmed again and filtered.
- The precipitate was washed with 1%  $\text{NH}_4\text{NO}_3$  solution and alumina content is estimate gravimetrically.
- The second filtrate contains CaO and MgO which could be estimated complexometrically with standard EDTA (**Ethylenediaminetetraacetic acid**) solution.



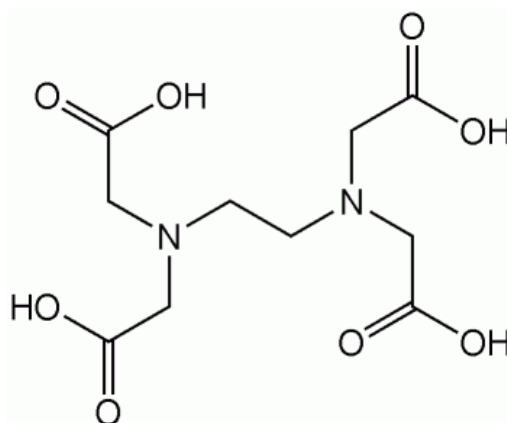


**Fig 2 EDTA structure**

- Finally loss of weight on ignition was determined by keeping about 0.4gm of sample in the furnace for 30 mins.

Fuse formation of china clay

1. Weight of china clay = 0.4922gm
2. Weight of  $\text{Na}_2\text{CO}_3$  = 10 gms
3. Number of NaOH bits = 4-5 bits
4. Rate of heating =  $3^\circ\text{C}$
5. Fusion temperature  $1000^\circ\text{C}$
6. Fusing time 1hour

### 3.2. Results of chemical analysis

- 1) Silica content = 52.2%
- 2)  $\text{Fe}_2\text{O}_3$  = 0.58 %
- 3)  $\text{Al}_2\text{O}_3$  = 33.01%
- 4)  $\text{CaO}$  = 1.88%
- 5)  $\text{MgO}$  = negligible
- 6) L.O.I = 12.4%

### 3.3. Calcination of China clay

Calcination of clay at  $1000^{\circ}\text{C}$  having a temperature rise of  $3^{\circ}\text{C}$  per minute and a soaking period two hours at  $1000^{\circ}\text{C}$ .

The sample is taken in a 500ml silimenite crucible. 400gms of china clay is taken in it and checked whether any agglomeration is there or not. Then the crucible is put inside the furnace.

### 3.4. Wet milling of calcined china clay (pot milling)

The milling and mixing of the calcined china clay is done in the silicon nitride ( $\text{Si}_3\text{N}_4$ ) crucible using  $\text{Si}_3\text{N}_4$  balls of two different sizes of balls. Distilled water is used as the wet medium. It is done for 5 hours. As this process is used for formation of high purity mullite formation so  $\text{ZrO}_2$  or steel balls are not used as they can contaminate the sample.



**Fig 3 Mixing of china clay in the pot mill**

### 3.5 Calculation of amount of Reactive Alumina content to form 100% mullite body

Formula for china clay is  $\text{Al}_2\text{O}_3 \cdot 2\text{SiO}_2 \cdot 2\text{H}_2\text{O}$

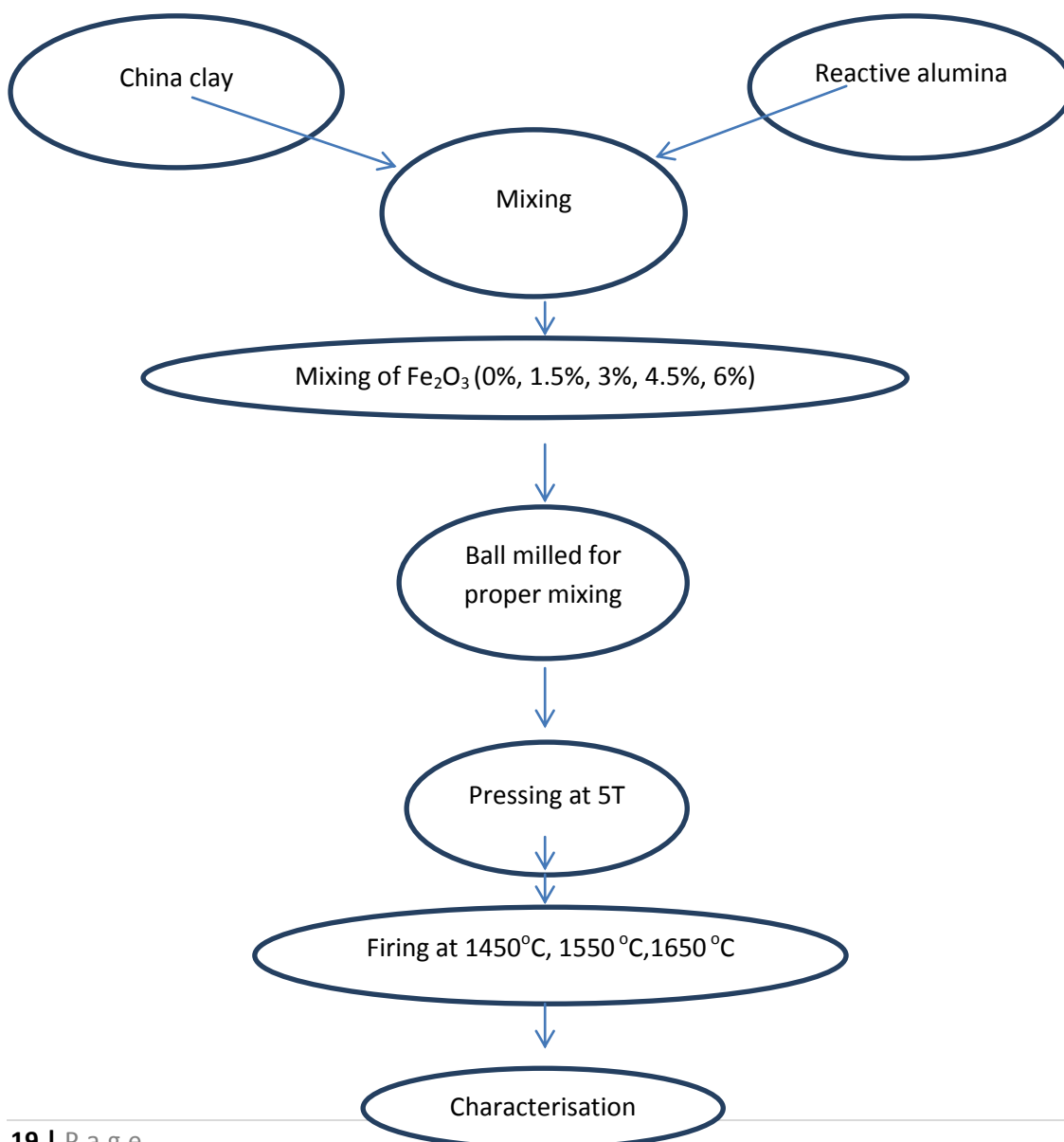
From chemical analysis we got 1 mole of china clay contains 33.01%  $\text{Al}_2\text{O}_3$ . Atomic weights of the elements are Al (27), Si (28), O (16) and H (1). From this we can calculate that from 258gm of china clay provides 102gm of alumina. Similarly from 100gm of china clay provides 39.534gm of alumina. From mathematical calculation we get

$$\frac{39.53 + x}{100 + x} = \frac{72}{100} \dots\dots\dots eq\ 1$$

$x$  is the amount of alumina to be added to the batch to give 100% mullite body.

From *eq 1* the value of  $x$  comes out 116gm. So the total batch comes out to be 216gm i.e to 100gm of china clay 116gm of reactive alumina is added.

### 3.6 Synthesis Flow chart



### 3.7 Batch preparation

Five batches of sample are prepared with different amount of  $\text{Fe}_2\text{O}_3$  varying from 0% to 6% with common difference of 1.5. As the LOI of china clay is 12.4% so 100gm of china clay is mixed with 116gm of reactive alumina.

- i. 100gm china clay + 116gm reactive alumina + 0%  $\text{Fe}_2\text{O}_3$  of the total batch
- ii. 100gm china clay + 116gm reactive alumina + 1.5%  $\text{Fe}_2\text{O}_3$  of the total batch
- iii. 100gm china clay + 116gm reactive alumina + 3%  $\text{Fe}_2\text{O}_3$  of the total batch
- iv. 100gm china clay + 116gm reactive alumina + 4.5%  $\text{Fe}_2\text{O}_3$  of the total batch
- v. 100gm china clay + 116gm reactive alumina + 6%  $\text{Fe}_2\text{O}_3$  of the total batch

### 3.8 Mixing of batches

The above batches are mixed for 1 hour with a rotational speed of 300rotation/min in the silicon nitride pot used previously. The mixed sample is taken out left for drying for 2days at a drier temperature of  $100^0\text{C}$ .



**Fig 4(a) Mixed sample**



**Fig 4(b) Dried sample after 2 days**

### **3.9 PVA solution preparation**

5gms of PVA (poly vynile alcohol) is added to distilled hot water slowly with constant stirring. Before heating the water, water level is marked. When water evaporates the beaker is filled to the marked level. The stirring is continued till a colourless solution is prepared. Similarly 300ml of PVA is prepared. Then all the bathces are mixed with around 20ml of PVA so that required green strength can be achieved after pressing. After mixing the samples are kept under the IR lamp so that all the moisture present can be dried.

### **3.10 Pressing**

For pallet preparation 0.8gm of sample are taken and pressed at 5T with a holding time of 2 mins in two stages. 2.5T is pressed and then held for 1minute then the pressure is rised to 5T and then held for 1min.

For brick preparation 30gm of the sample is taken and pressed at 8T similarly in two stages as expressed above.

12 pallets and 6 bricks of every batch is pressed and then they are fired at 3 different temperatures.

### **3.11 Firing**

As the sample contains silica and we know it has displasive phase transformation in the temperature range  $500^{\circ}\text{C}$  so extra care has been taken during firing. Sample also contains PVA which completely burns out at  $450^{\circ}\text{C}$ . So the temperature is slowly increased at a rate of  $3^{\circ}\text{C}$  per minute till the temperature rises to  $500^{\circ}\text{C}$ . There the temperature is held for 1 hour to accommodate the transformation and complete binder burnout. The temperature is then rised to  $1000^{\circ}\text{C}$  at a rate of  $3^{\circ}\text{C}$  to accommodate the further displasive transfromation in the silica phases. Then the temperature is rised at a rate of  $5^{\circ}\text{C}$  till the temperature is

reaches required temperature. The batches are firer at  $1450^{\circ}\text{C}$ ,  $1550^{\circ}\text{C}$ ,  $1650^{\circ}\text{C}$ . some of the fired samples pictures are shown in the following picture.

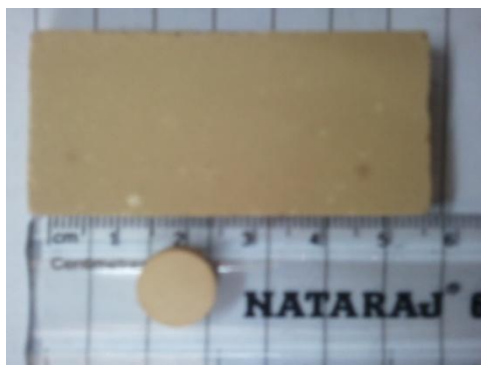


Fig5 Fired sample picture

# CHAPTER 4

## EXPERIMENTAL

## CHARACTERISTIC

#### 4.1 DSC and TG of the China Clay

The DSC/ TG experiments were conducted in a Netzsch 449C Thermal Analyser. The samples were heated in flowing Ar gas atmosphere at a heating rate of 5°C/min and 10°C/min. The weight loss measurements were also done in the same instrument and the results are shown in Figure 7.

#### 4.2 Bulk density and Apparent porosity measurement

To measure bulk density and apparent porosity of sample pellets, first the dry weight of pellets was measured. Then they were soaked in distilled water kept inside a beaker and is boiled till all the air bubbles vanished. After that they were kept inside vacuum for few hours. After removing from vacuum the suspended weight and soaked weight of the samples were calculated.

To obtain bulk density (B.D.) the following formula was used:

$$\text{B.D.} = \frac{(\text{dry weight})}{(\text{soak weight} - \text{suspended weight})} \dots\dots\dots \text{eq2}$$

$$\text{A.P.} = \frac{(\text{soak weight} - \text{dry weight})}{(\text{soak weight} - \text{suspended weight})} \times 100 \dots\dots\dots \text{eq 3}$$

The plots of the bulk density vs temperature and bulk density vs % Fe<sub>2</sub>O<sub>3</sub> are shown in the figure 8 and 9. Similarly AP vs temperature and AP vs Fe<sub>2</sub>O<sub>3</sub> are shon in the figure 10 and 11.

#### 4.3 Linear shrinkage

The dimensions of the unfired body are measured and then the dimensions of fired are measured. Then by subtracting final length from the initial length we get the linear shrinkage. To get the percentage linear shrinkage value we use the following formula:

$$\% \text{Linear shrinkage} = \frac{\text{initial lenght} - \text{final lenght}}{\text{final lenght}} \times 100 \dots\dots\dots \text{eq 4}$$



The plot of the %linear shrinkage vs temperature and % linear shrinkage vs %Fe<sub>2</sub>O<sub>3</sub> is shown in the figure 12 and 13.

#### 4.4 BET surface area

The BET surface area is done of the calcined china clay to calculate the particle size of the calcined china clay.

$$\text{Particle size (D)} = \frac{6}{\phi d} \dots \dots \dots \text{eq 5}$$

Where  $\phi$  is the surface area and  $d$  is the density of the particle. The BET plot is shown in the figure 14.

#### 4.5 Cold crushing strength of the samples

The Biaxial Tensile Strength of the pellets were measured by breaking the samples in a Tinius Olsen Materials Testing Machine (HK10S model) was used. It has a maximum load cell capacity of 10 KN. The biaxial tensile strength,  $S$  was obtained using the formula:

$$S = \frac{(2 * P)}{(\pi * D * t)} \dots \dots \dots \text{eq 6}$$

Where  $P$  ⇨ Maximum Load

$D$  ⇨ Diameter of the pellet

$t$  ⇨ Thickness of the pellet

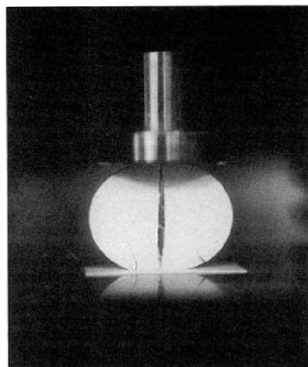


**Fig 6 Diametric compression test (loading and fracture mode)**

#### **4.6 XRD analysis**

XRD analysis of the raw material and the selected fired samples are done. XRD is done to know the sample purity, percentage mullite formation and crystallite size variation and the growth direction.

#### **4.7 SEM analysis**

SEM analyses of the selected samples are done to know about the grain size and grain size variation with the variation in the composition at temperature 1650<sup>0</sup>C. The sample are mounted on the sample holder and put inside the SEM.

# CHAPTER 5

## RESULT AND DISCUSSION

## 5.1 DSC/TG Graph

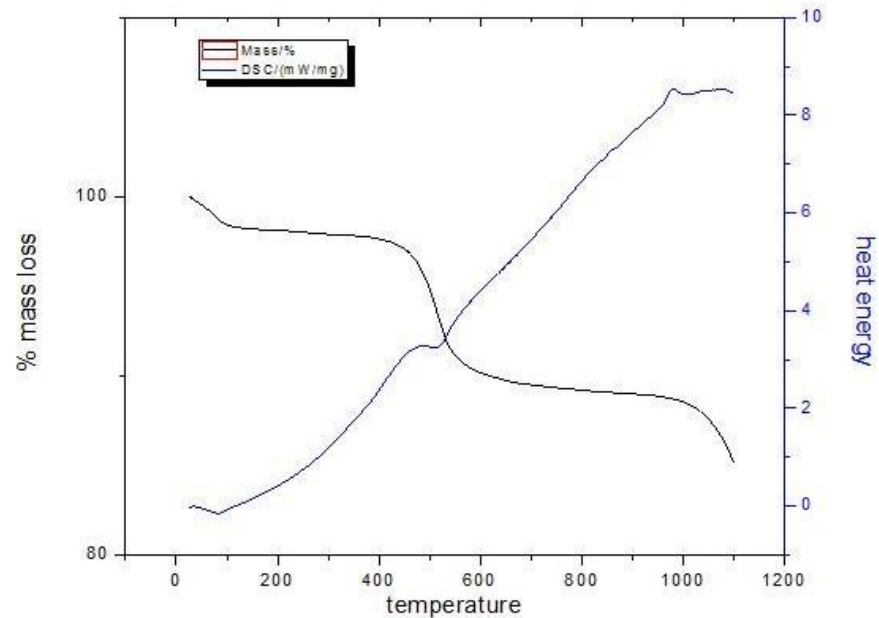


**Fig 7 DSC and TG plot of the china clay**

From the figure 7 we can see that:

- ❖ At temperature around 100 °C the endothermic peak is due to the release of the absorbed water in the clay
- ❖ The endothermic peak at 520°C is due to the release of the lattice water present in the clay.
- ❖ At around 980°C an exothermic peak is may be due to a) Spinel formation b) 2:1 mullite formation <sup>[18]</sup>.

## 5.2 Density of the samples

As the temperature increases the density increases after 1550<sup>0</sup>C there is sudden increase in the density because of the increase in the reaction rate of the transitory liquid phase present and the excess reactive alumina added to the sample.

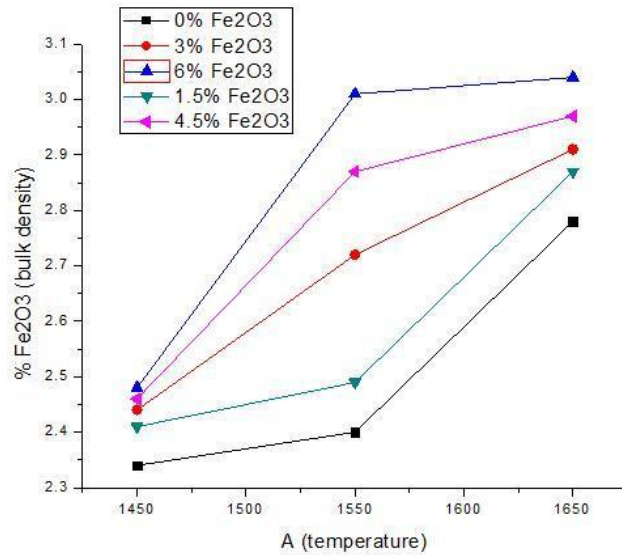


**Fig 8 Bulk density vs Temperature**

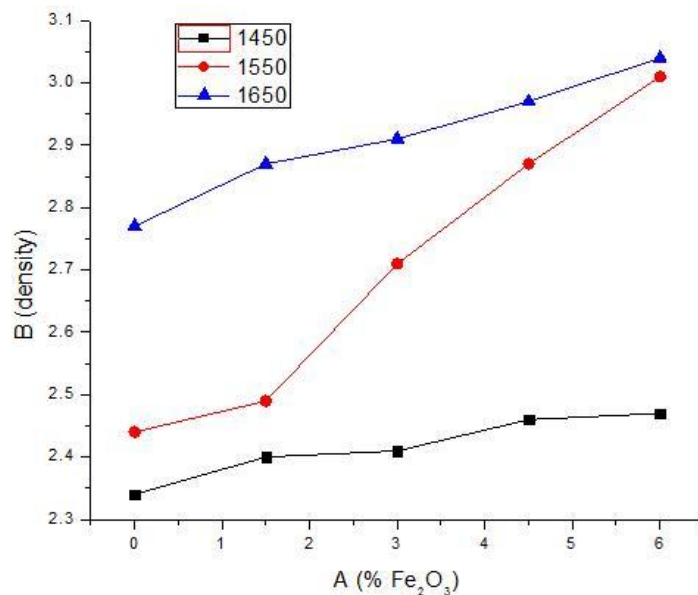


**Fig 9 Bulk density vs % Fe<sub>2</sub>O<sub>3</sub>**

As we can see from the figure 8 & 9 the maximum density achieved is 3.04 for the sample with 6% Fe<sub>2</sub>O<sub>3</sub> fired at 1650<sup>0</sup>C. The percentage density achievement of the sample to the

true density is 96%. The reason may be due to the presence of free iron oxide present in the system. The rapid increase in the density is due to the replacement of the  $Al^{+3}$  ion from its regular octahedral site by  $Fe^{+3}$  and the free  $Al^{+3}$  replaces the  $Si^{+4}$  from its regular tetrahedral site. So increase in the amount of  $Fe_2O_3$  content there is increase in the reaction between the silica and alumina and formation of mullite.

### 5.3 Apparent Porosity in the sample

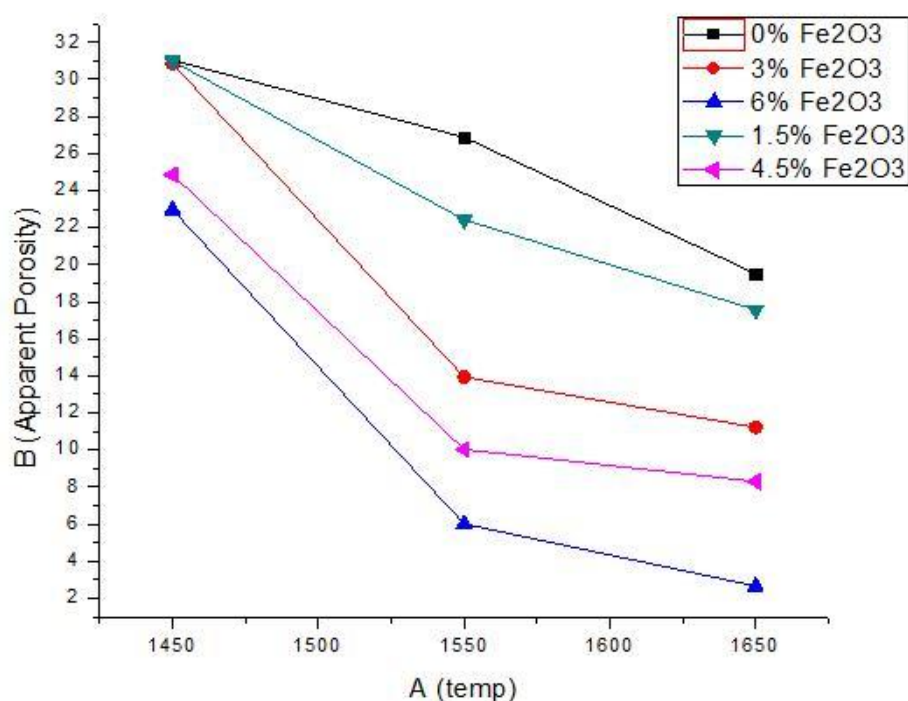


**Fig 10 AP vs temperature**

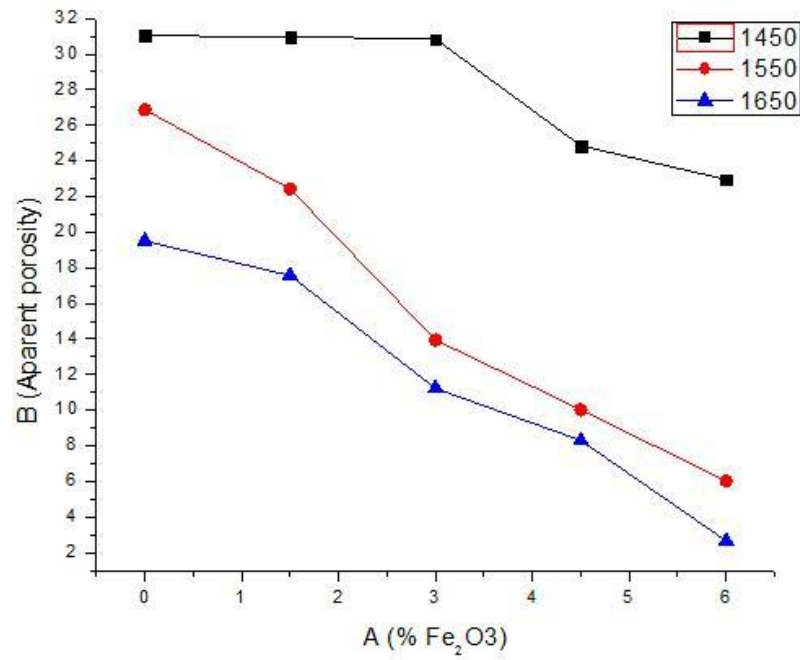


**Fig 11 AP vs % Fe<sub>2</sub>O<sub>3</sub>**

The minimum porosity is shown by the sample 6% Fe<sub>2</sub>O<sub>3</sub> fired at 1650°C (Fig 10 & Fig 11).

There is decrease in the porosity level as there is increase in the Fe<sub>2</sub>O<sub>3</sub>.

#### 5.4 Linear shrinkage

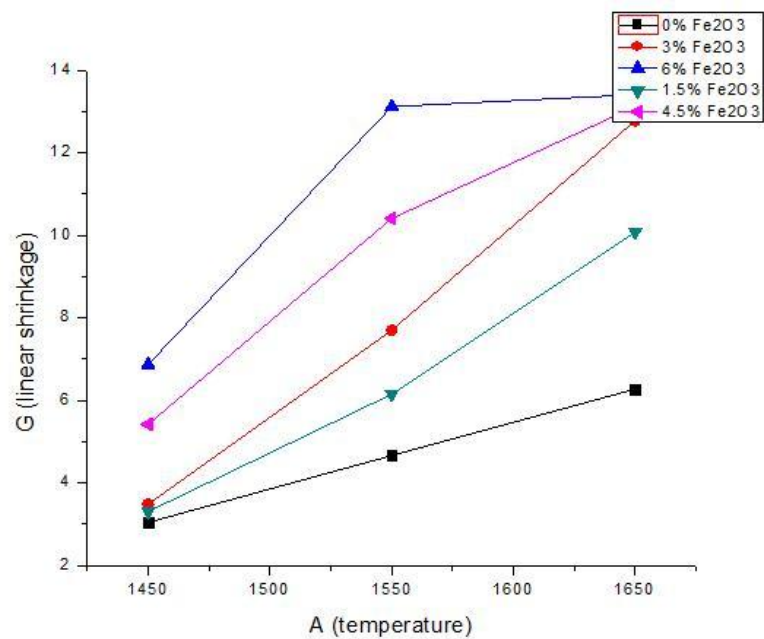


**Fig 12 Linear shrinkage vs Temperature**

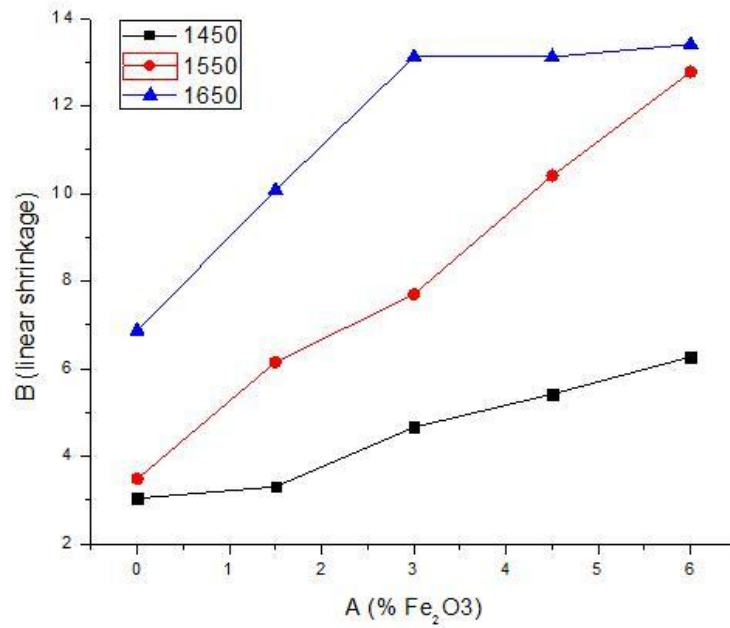


**Fig 13 linear shrinkage vs % Fe<sub>2</sub>O<sub>3</sub>**

As from the figure 12& 13 the maximum linear shrinkage is shown by the sample which shows maximum density i.e equal to 13.41%. The linear shrinkage could have been more if there raw clay instead of calcined clay has been used.

### 5.5 BET surface area analysis



**Fig 14 BET surface area plot**



From the formula

$$\text{Particle size (D)} = \frac{6}{\phi d}$$

$$\Phi = 8.22 \text{ m}^2/\text{gm} \text{ (Fig 14)}$$

## 5.6 CCS analysis of the samples

CCS(MPa) TEMP	0% Fe <sub>2</sub> O <sub>3</sub>	1.5% Fe <sub>2</sub> O <sub>3</sub>	3% Fe <sub>2</sub> O <sub>3</sub>	4.5% Fe <sub>2</sub> O <sub>3</sub>	6% Fe <sub>2</sub> O <sub>3</sub>
1450 <sup>0</sup> C	89.04	94.60	99.03	97.18	99.00
1550 <sup>0</sup> C	101.44	89.08	89.00	92.56	96.06
1650 <sup>0</sup> C	123.37	97.00	86.03	90.41	92.07

With 0% Fe<sub>2</sub>O<sub>3</sub> there are some amount of free alumina. Due to presence of unreacted alumina the sample shows higher CCS strength and as the mullite formation amount increases i.e with increase in the Fe<sub>2</sub>O<sub>3</sub> content there is decrease in the CCS.

## 5.7 XRD analysis raw materials

XRD analysis of the calcined china clay and reactive alumina is done. From the XRD plot we can see that there are peaks of alumina silicate of the calcined clay as shown in the figure 15. In the reactive alumina peak all the peaks of the alumina are matching as shown in the figure 16.

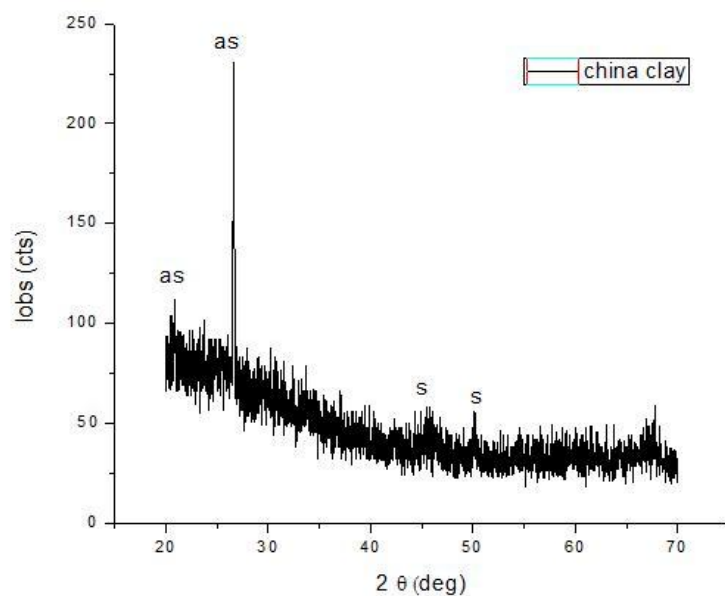


**Fig 15 XRD of china clay calcined at 1000<sup>0</sup>C**

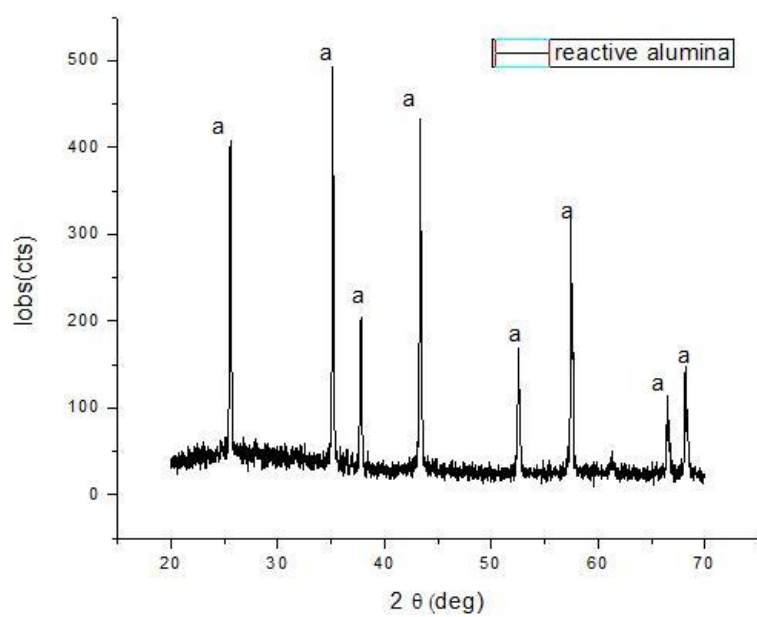


**Fig 16 XRD of reactive alumina**

## 5.8 XRD analysis fired sample

XRD analysis of some of the selected fired sample are done. Sample which are fired at  $1650^{\circ}\text{C}$  with a doping of 0%, 3%, 4.5%, 6%  $\text{Fe}_2\text{O}_3$ . The XRD plot of the sample are plotted in the following figures.

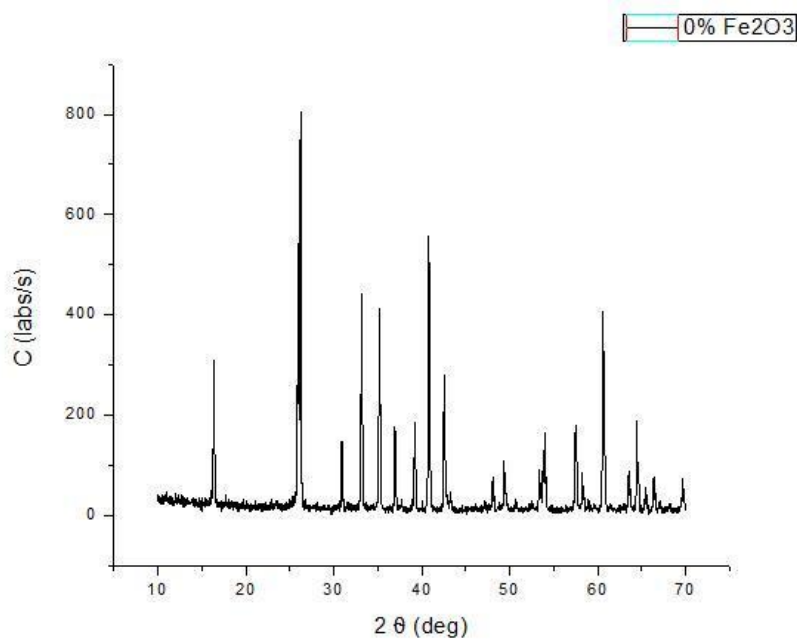


**Fig 17 XRD analysis of the 0%  $\text{Fe}_2\text{O}_3$  ( $1650^{\circ}\text{C}$ )**

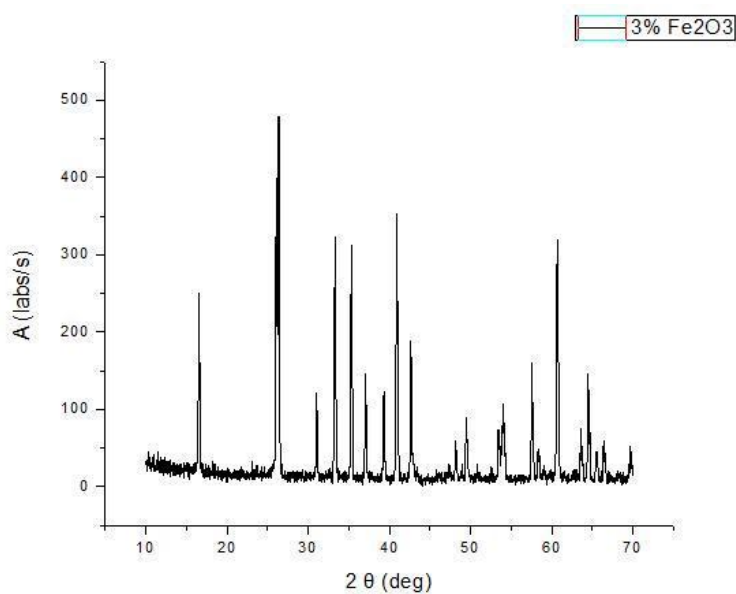


**Fig 18 XRD analysis of the 3%  $\text{Fe}_2\text{O}_3$  ( $1650^{\circ}\text{C}$ )**

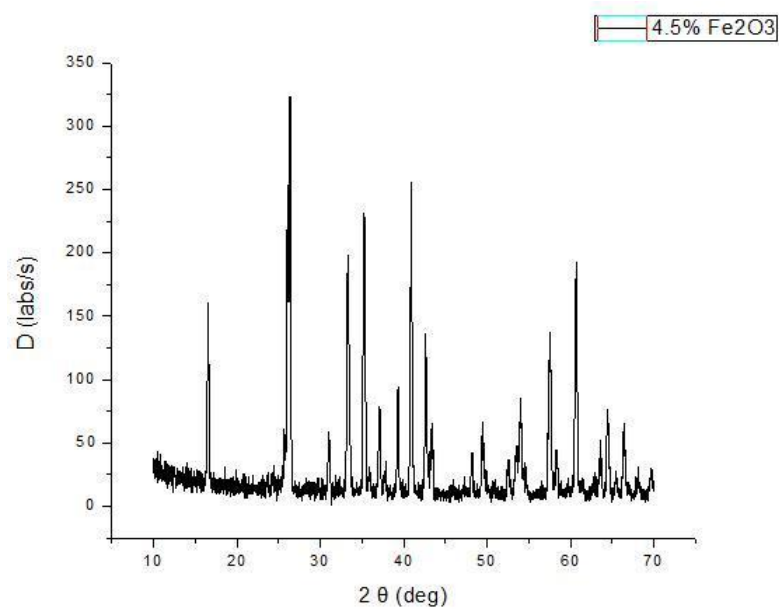


**Fig 19 XRD analysis of the 4.5% Fe<sub>2</sub>O<sub>3</sub>(1650<sup>0</sup>C)**

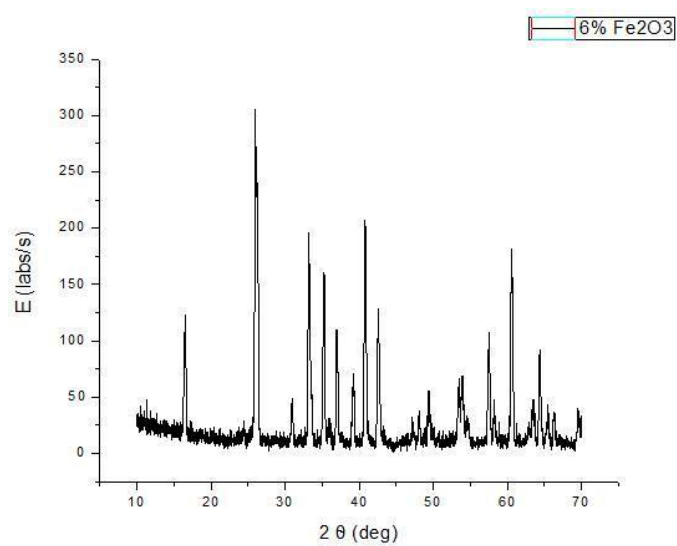


**Fig 20 XRD analysis of the 6% Fe<sub>2</sub>O<sub>3</sub>(1650<sup>0</sup>C)**

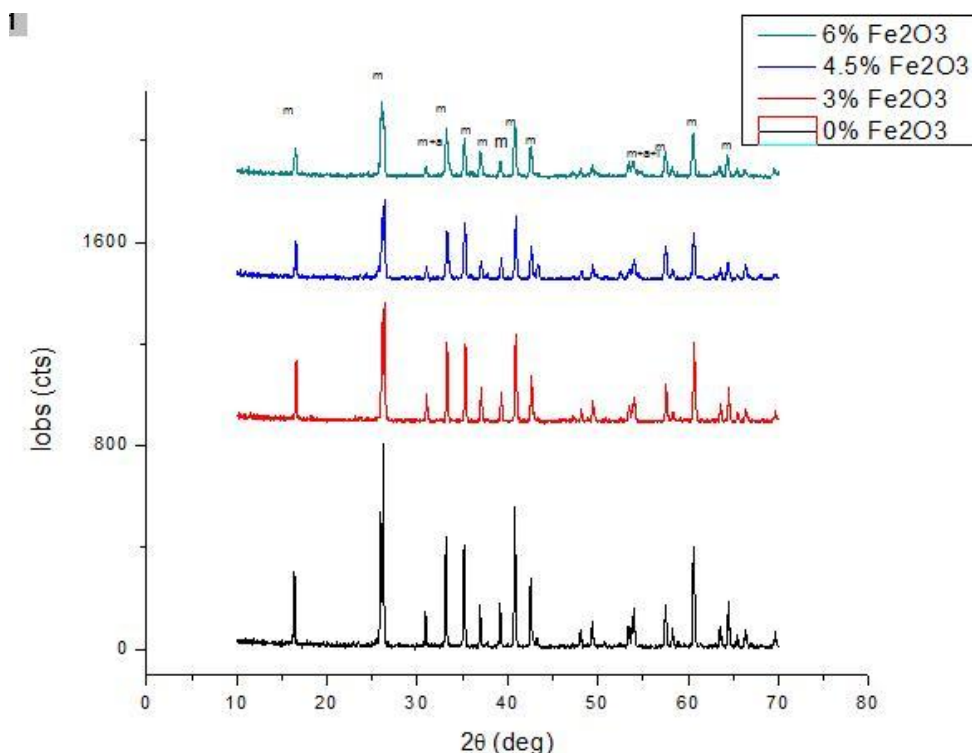


**Fig 21 XRD analysis of 0% Fe<sub>2</sub>O<sub>3</sub>, 3% Fe<sub>2</sub>O<sub>3</sub>, 4.5% Fe<sub>2</sub>O<sub>3</sub>, 6% Fe<sub>2</sub>O<sub>3</sub> fired at 1650<sup>0</sup>C**

From fig-17 to fig-20 it can be said that there is some free amount of alumina present in the samples with 0% Fe<sub>2</sub>O<sub>3</sub>, 3% Fe<sub>2</sub>O<sub>3</sub> and 4.5% Fe<sub>2</sub>O<sub>3</sub>. But there has been total elimination of the alumina peak with sample composition 6% Fe<sub>2</sub>O<sub>3</sub>. The percentage mullite formation can be calculated by the following formula:

$$\frac{\text{total mullite peak area}}{\text{total peak area}} \times 100$$

From the above formula when calculated the percentage mullite formation found in the samples are

- 0% Fe<sub>2</sub>O<sub>3</sub> = 98.0581% (Fig 17)
- 3% Fe<sub>2</sub>O<sub>3</sub> = 99.28 % (Fig 18)
- 4.5% Fe<sub>2</sub>O<sub>3</sub> = 98.41% (Fig 19)
- 6% Fe<sub>2</sub>O<sub>3</sub> = 98.39% (Fig 20)

With 6%  $\text{Fe}_2\text{O}_3$  there is total elimination of alumina peak but there are appearance of some iron oxide peak with negligible intensity. From the above graph (Fig 21) we see that there is decrease in the intensity of the peaks as there is rise in the % $\text{Fe}_2\text{O}_3$  content. Which signifies the crystalite size is decreasing with increasing % $\text{Fe}_2\text{O}_3$  content.

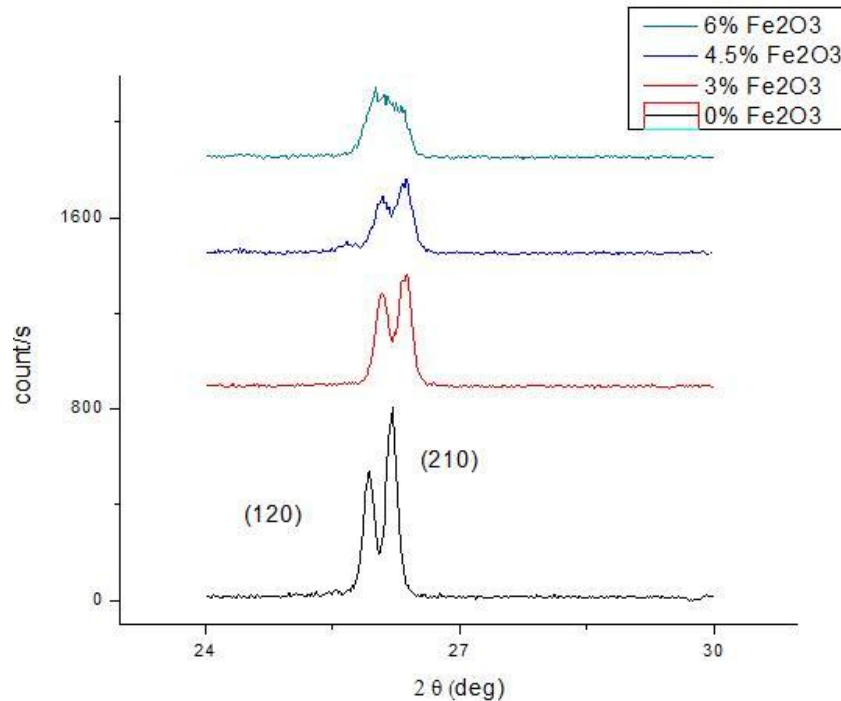


**Fig 22 XRD analysis of 0%  $\text{Fe}_2\text{O}_3$ , 3%  $\text{Fe}_2\text{O}_3$ , 4.5%  $\text{Fe}_2\text{O}_3$ , 6%  $\text{Fe}_2\text{O}_3$  samples fired at  $1650^\circ\text{C}$  are plotted in range  $2\theta$  (25-30)**

From the Fig 22 we can see that there is relative intensity increase in the diffracted rays coming from the plane (120) with respect to the plane (210). So we can say that the grain growth takes place in the (120) plane.

### 5.9 SEM analysis

The samples containing of 0%  $\text{Fe}_2\text{O}_3$ , 3%  $\text{Fe}_2\text{O}_3$ , 4.5%  $\text{Fe}_2\text{O}_3$ , 6%  $\text{Fe}_2\text{O}_3$  samples fired at  $1650^\circ\text{C}$  are chosen for SEM analysis. From the SEM images we can clearly see that there is formation of  $1\mu\text{m}$  mullite grains as shown in the Fig 23(a). From the SEM images of the 3%  $\text{Fe}_2\text{O}_3$  sample we can see that the grain size has been increased to  $3\text{--}4\mu\text{m}$  (Fig 24) but in both the

cases the aspect ratio of the mullite grain. From the SEM images of the 4.5%  $\text{Fe}_2\text{O}_3$  we see that the grain size has been increased to  $5\mu\text{m}$  as shown in the Fig 25(a). But in this image we see that the needle like mullite grains are forming. Similarly we see in the Fig 26 the mullite grain size has been increased to  $10\mu\text{m}$  with prominent needle like structure for the sample 6%  $\text{Fe}_2\text{O}_3$ . The aspect ratio of this sample is very high in comparison to the others.

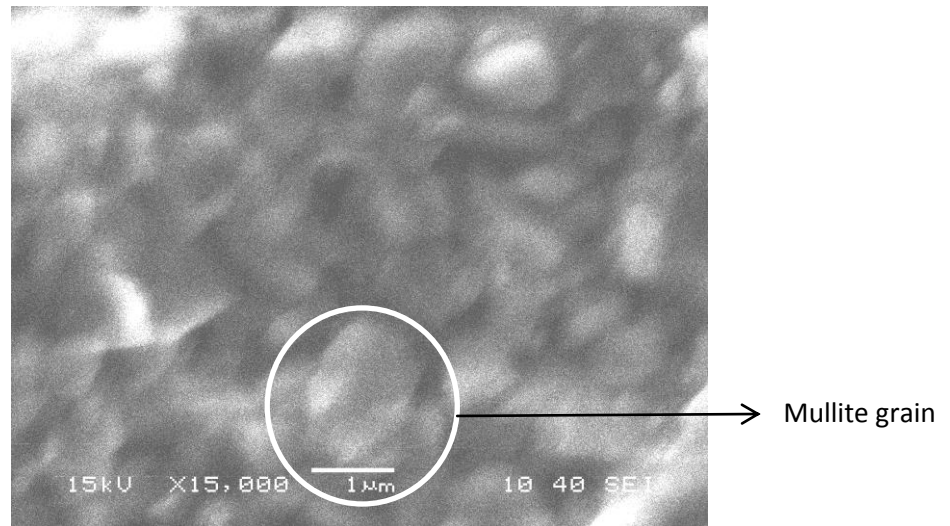


**Fig 23(a) SEM image of 0%  $\text{Fe}_2\text{O}_3$  (X15000)**

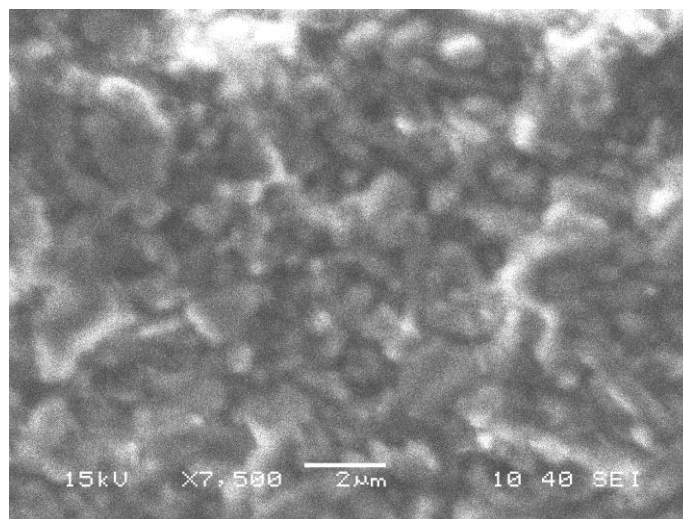


**Fig 23(b) SEM image of 0%  $\text{Fe}_2\text{O}_3$  (X7500)**

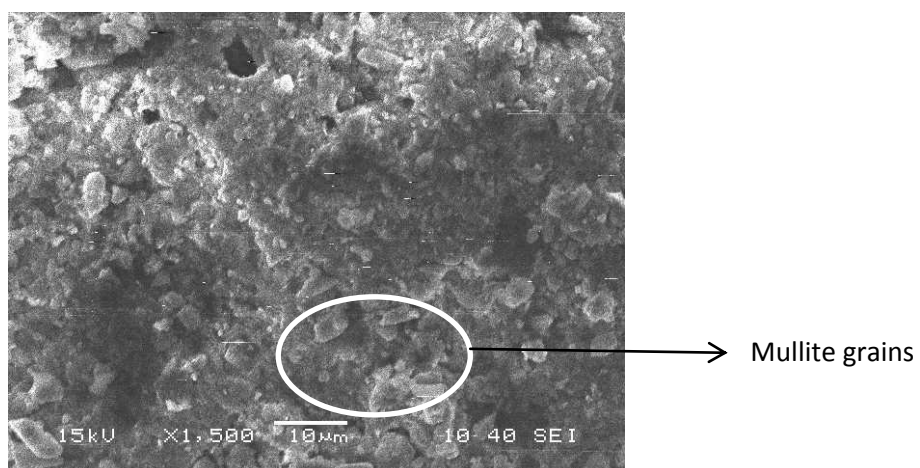


**Fig 24 SEM image of 3%  $\text{Fe}_2\text{O}_3$ (X1500)**

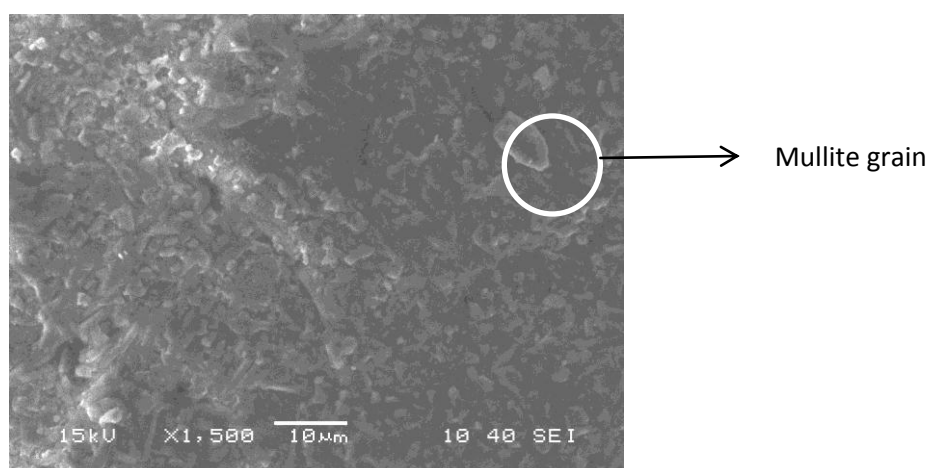


**Fig 25(a) SEM image of 4.5%  $\text{Fe}_2\text{O}_3$ (X1500)**

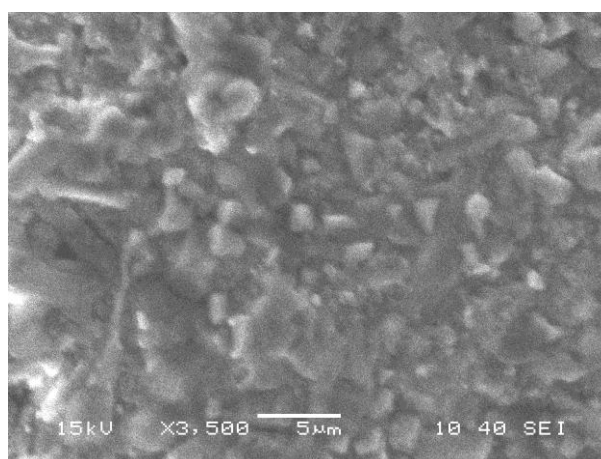


**Fig 25(b) SEM image of 4.5%  $\text{Fe}_2\text{O}_3$ (X3500)**



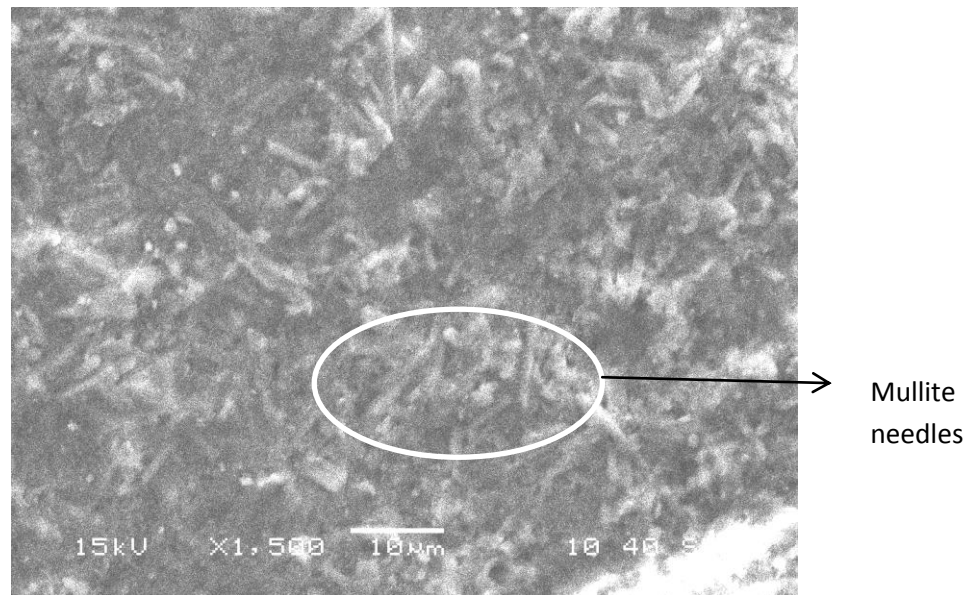


**Fig 26 SEM image of 6%  $\text{Fe}_2\text{O}_3$ (X1500)**

# CHAPTER 6

# CONCLUSION

## Conclusion

- From all the batches fired at 1650<sup>0</sup>C there is formation of mullite more than 98%.
- With 3% Fe<sub>2</sub>O<sub>3</sub> we get the maximum mullite formation i.e. 99.28%.
- There are traces of unreacted alumina in the sample of 0% Fe<sub>2</sub>O<sub>3</sub>, 3% Fe<sub>2</sub>O<sub>3</sub> and 4.5% Fe<sub>2</sub>O<sub>3</sub> and the intensity is decreasing with % Fe<sub>2</sub>O<sub>3</sub> content.
- With 6% Fe<sub>2</sub>O<sub>3</sub> we get 98.39% mullite formation with traces of iron oxide but there is no sign of unreacted alumina which suggests the complete conversion of unreacted alumina to mullite.
- From the SEM figures we see that even though all the samples fired at 1650<sup>0</sup>C gives mullite but there is variation in their grain size. With 0% Fe<sub>2</sub>O<sub>3</sub> we get smallest (2μm) grain size, with 3% Fe<sub>2</sub>O<sub>3</sub> we get 3-4μm and the aspect ratio of both the above samples are very poor but with 4.5% Fe<sub>2</sub>O<sub>3</sub> the grain size increases to 5μm and there is improvement in their aspect ratio and with 6% Fe<sub>2</sub>O<sub>3</sub> we get needle like structure with highest aspect ratio and a grain size of 10μm.
- The crystal growth takes place in the (120) plane as there is rise in the intensity of the (120) plane with respect to the (210) plane.

# CHAPTER 7

## SCOPE FOR FUTURE WORK

- XRD analysis of the entire sample fired at 1450<sup>0</sup>C and 1550<sup>0</sup>C should be carried out.
- SEM analysis of the entire sample fired at 1450<sup>0</sup>C and 1550<sup>0</sup>C should be carried out.
- Batches should be fired at different soaking period and characterised.
- Thermal shock resistance should be calculated for all the batches and
- Corrosion test should be done for all the batches.

## References

1. Effect of Fluoride and Oxide Additives on the Phase Transformations in Alumina/Clay Ceramics, N.Tezuka , I. M. Low , I. J. Davies , I. D. Alecu , R. J. Stead E. G. Mehrtens and B. A. Latella (American ceraimc society)
2. Solubility of  $\text{Fe}_2\text{O}_3$ ,  $\text{TiO}_2$ ,  $\text{MgO}$  in millite, H. Schneider (ceramic international 13 (1987) 77-82)
3. Iron incorporation in mullite, H. Schneider (ceramic international 12 (1986) 177-125)
4. Fabrication and characterization of highly porous mullite ceramics, J.H. She\*, T. Ohji (Materials Chemistry and Physics 80 (2003) 610–614)
5. Mullite Precursor Phases, H. Schneider, B. Saruhan, D. Voll (*Journal of the European Ceramic Society* 11 (1993) 87 94)
6. Synthesis and structural characterization of non-crystalline mullite precursors, H. Schneider, D. Voll, B. Saruhan , J. Sanz , G. Schrader , C. Riischer , A. Mosset (Journal of Non-Crystalline Solids 178 (1994) 262-271)
7. Mullitization behavior of calcined clay- alumina mixtures, V. Viswabaskaran, F.D. Gnanam, M. Balasubramanian . Ceramic international 29 (2003) 561-571
8. S. Somiya and Y. Hirata, “Mullite Powder Technology and Applications in Japan”, Am. Ceram. Soc. Bull., Vol.[**70**], 10, (1991), 1624-1632
9. C.Y. Chen, G.S. Lan, and W.H. Tuan, "Preparation of mullite by the reaction sintering of kaolinite and alumina", J. Eur. Ceram. Soc., Vol. [**20**], 14-15, (2000), 2519-2525
10. H.S. Tripathi, S. Kr Das, and G. Banerjee, "Thermal shock behaviour of high alumina aggregates derived from sillimanite beach sand with and without  $\text{Fe}_2\text{O}_3$  doping", Ceram. Int., Vol. [**26**], 1, (2000), 1-6

11. K. Okada and N. Otuska, "Synthesis of Mullite Whiskers and Their Application in Composites", Journal of American Ceramic Society. Vol. [74], 10, (1991), 2414-2418.
12. K. Ishizaki, S. Komarneni, M. Nanko, Porous Materials: Process Technology and Applications, Kluwer Academic Publishers, Dordrecht, 1998.
13. J.D. Heaps, S.B. Schuldt, B.L. Grung, J.D. Zook and C.D. Butter, IEEE Proc., 30th Elec. Comp. Conf. (1980) 39-48.
14. Thermal expansion of mullite, journal of American ceramic society 73 (1990) 2073-2076
15. W.E. Lee, W.M. Rainforth, Ceramic microstructure, Property control by processing Chapman and Hall, London, UK, 1994, pp. 299-311
16. D.S. Perera and G. Allott, "Mullite Morphology in Fired Kaolinite/halloysite Clays", J. Mater. Sci. Lett., Vol. [4], (1985), 1270-1272.
17. Mullitization behaviour of south Indian clays, V. Viswabaskaran, F.D. Gnanam, M. Balasubramanian. Ceramic international 28(2002) 557-564.
18. Mullite formation in Kaolinite – $\alpha$ -alumina, Kuo chung liu, G. Thomas, J.S. Moya.
19. XRD microstructure analysis of mullites obtained from Kaolinite-alumina mixtures, M.A. Sainz, F.J. Serrano, J.M. Amigo, J. Bastida, A. Caballera .

